Nucleic Acids Research, 2005, Vol. 33, No. 6 ***1749–1759***
doi:10.1093/nar/gki318

Solution structure of a modified 2′,5′-linked RNA hairpin involved in an equilibrium with duplex

Miha Plevnik, Zofia Gdaniec[1] and Janez Plavec*

Slovenian NMR Center, National Institute of Chemistry, Hajdrihova 19, PO Box, 660, SI-1001 Ljubljana, Slovenia and [1]Institute of Bioorganic Chemistry, Polish Academy of Sciences, Noskowskiego 12/14, 61-704 Poznan, Poland

Received December 21, 2004; Revised February 2, 2005; Accepted March 2, 2005 Protein Data Bank accession ID 1XV6

ABSTRACT

The isomerization of phosphodiester functionality of nucleic acids from 3′,5′- to a less common 2′,5′-linkage influences the complex interplay of stereoelectronic effects that drive pseudorotational equilibrium of sugar rings and thus affect the conformational propensities for compact or more extended structures. The present study highlights the subtle balance of non-covalent forces at play in structural equilibrium of 2′,5′-linked RNA analogue, 3′-*O*-(2-methoxyethyl) substituted dodecamer *CG*CGAA*U*U*CG*CG, 3′-MOE-2′,5′-RNA, where all cytosines and uracils are methylated at C5. The NMR and UV spectroscopic studies have shown that 3′-MOE-2′,5′-RNA adopts both hairpin and duplex secondary structures, which are involved in a dynamic exchange that is slow on the NMR timescale and exhibits strand and salt concentration as well as pH dependence. Unusual effect of pH over a narrow physiological range is observed for imino proton resonances with exchange broadening observed at lower pH and relatively sharp lines observed at higher pH. The solution structure of 3′-MOE-2′,5′-RNA hairpin displays a unique and well-defined loop, which is stabilized by Watson–Crick A5·*U8 base pair and by $n \rightarrow \pi^*$ stacking interactions of O4′ lone-pair electrons of A6 and *U8 with aromatic rings of A5 and *U7, respectively. In contrast, the stem region of 3′-MOE-2′,5′-RNA hairpin is more flexible. Our data highlight the important feature of backbone modifications that can have pronounced effects on interstrand association of nucleic acids.

INTRODUCTION

Most of the naturally occurring nucleic acids consist of nucleotide chains where 3′ and 5′ functionalities of two neighboring nucleotides are connected by the phosphodiester group. One of the interesting puzzles is why nature has chosen 3′,5′-phosphodiester linkage along sugar-phosphate backbone over the 2′,5′ analogue. Several experimental and theoretical studies have addressed this subject (1–9). However, this field of nucleic acids is not fully explored and many questions still remain to be answered. The isomerization from 3′- to 2′-phosphodiester linkage together with other substituents on the sugar ring including heterocyclic moiety are involved in the interplay of stereoelectronic effects that drive sugar pseudorotational equilibrium and, therefore, influence the conformational propensities of nucleic acids for A- or B-type structure. In this way, intermolecular association of single strands could be facilitated through engineered structural preorganization of individual oligonucleotide strands that is achieved by the choice of substituents on ribofuranosyl moiety. Switching between axial and equatorial orientations of phosphate groups also defines the relative positions and distances between nucleobases, which affects stabilization of a folded functional three-dimensional (3D) structure by stacking interactions between heterocyclic moieties themselves and with sugar-phosphate backbone.

It is known that 2′,5′-linked RNAs are intimately associated with a wide variety of biological functions which warrants that further structural studies are needed to understand the molecular basis of their functions. In order to gain insight into the origins of conformational properties of 2′,5′-linked RNAs we have conducted a spectroscopic study on a model molecule, RNA analogue, 3′-MOE-2′,5′-RNA. All cytosine and uracil residues of a fully 3′-*O*-(2-methoxyethyl) modified 5′-*CG *CGAA*U*U*CG*CG-2′ dodecamer are methylated at position C5. The sequence of the modified 2′,5′-linked molecule (Figure 1a) is equivalent to the 3′,5′-linked 2′-deoxyribo analogue d(CGCGAATTCGCG)$_2$, whose structure has been investigated in detail by using X-ray crystallography and NMR spectroscopy, both in deoxy- and ribo- series (10–12). Through the years this so-called Dickerson–Drew sequence serves as a benchmark for both experimental and theoretical studies. The present spectroscopic study on 2′,5′-linked

*To whom correspondence should be addressed. Tel: +386 1 47 60 353; Fax: +386 1 47 60 300; Email: janez.plavec@ki.si

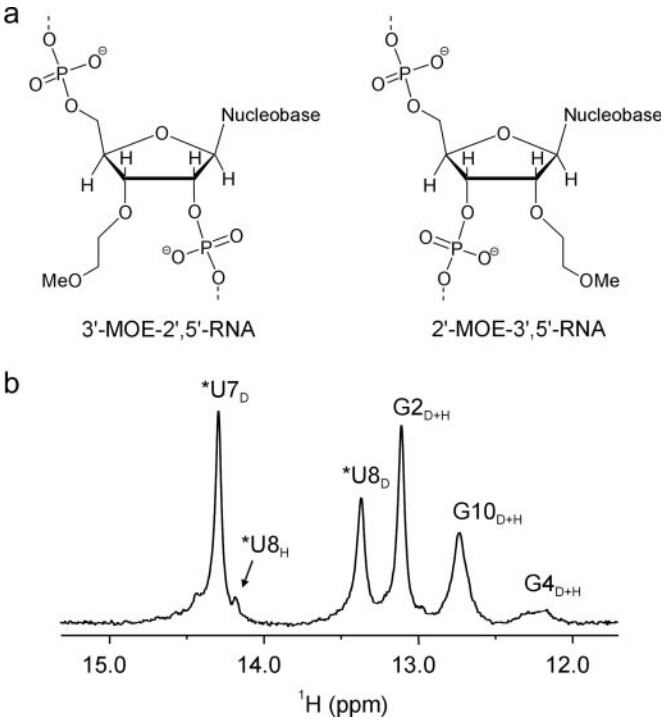

Figure 1. Non-terminal building blocks of 2′,5′- and 3′,5′-linked RNAs and imino proton spectra of 3′-MOE-2′,5′ RNA. (**a**) Shematic representation of 3′-MOE-2′,5′-RNA monomer (left) and 2′-MOE-3′,5′-RNA monomer (right). (**b**) Imino proton spectrum recorded in 90% H_2O/10% ^2H_2O at 9.0 mM strand concentration, 50 mM NaCl, pH 6.9 and 20°C. Duplex (D) and hairpin (H) resonances are denoted.

palindromic sequence reveals the presence of a hairpin in an equilibrium with a duplex and describes equilibrium dependences on oligomer and salt concentrations as well as pH changes. Although the hairpin loop is one of the most commonly observed RNA structural motifs (13), very little is known about the structural RNA motifs containing 2′,5′-phosphodiester linkages. Here, we report the NMR solution structure of 2′,5′-linked hairpin that represents, to the best of our knowledge, the first high resolution structure of a fully 2′,5′-linked RNA hairpin in solution. Our findings complement previous reports on stabilizing effects of 2′,5′-linkages on hairpin formation (14,15). At the same time, our results oppose traditional view of RNA hairpins in which the stem is considered to be highly structured while the loop is disordered.

METHODS

NMR spectroscopy

NMR spectra of 3′-MOE-2′,5′-RNA dodecamer were recorded on using Varian Unity INOVA 600 MHz spectrometer at different oligomer concentrations (0.2–9.0 mM), pH values (6.0–8.3) and NaCl concentrations (50, 100 and 350 mM) in the temperature range from 0 to 80°C in either 100% ^2H_2O or 90% H_2O/10% ^2H_2O. All the data used as restraints in structure determination were obtained at 0.9 mM strand concentration, 50 mM NaCl, 10 mM sodium phosphate buffer at pH* 7.4 and 30°C. ^1H, ^{13}C and ^{31}P assignments were obtained by using standard homonuclear and heteronuclear methods (16). The H2 resonances of two adenine residues were identified from their long T_1 values as compared with other protons. Translational diffusion constants (D_T) of the 3′-MOE-2′,5′-RNA oligomer and reference 2′-MOE-3′,5′-RNA oligomer (12mer duplex of the same sequence and base modifications but with different phosphodiester linkage) were measured at 25°C with the help of pulse-field gradient (PFG) NMR experiments according to the equation: $\ln(A') = -(\gamma\delta g)^2(\Delta - \delta/3)D_T + \ln(A_0)$ (17), where A' and A_0 are the measured peak intensities with and without applying PFG, respectively, γ is the gyromagnetic ratio, δ is the duration of PFG pulse, g is the strength of PFG and Δ is the delay time between the two PFG pulses in BPPSTE pulse sequence (18). D_T values of the 3′-MOE-2′,5′-RNA oligomer were determined in the solution of hairpin–duplex mixture and resolved resonances were used in the calculations. Measurements at lower strand concentration, where hairpin was predominant afforded identical D_T values for hairpin form. Spectra were processed and analyzed using VNMR 6.1B (Varian Inc.) and FELIX 2000 software (Accelrys Inc.).

Structure calculations

Distance restraints between non-exchangeable protons were obtained from a 2D NOESY in ^2H_2O at 30°C acquired with a 200 ms mixing time, which was verified to be within the linear range of NOE buildup curves. NOE distances were calibrated using C7(H7)$_3$–H6 distances (2.7 Å) of C5-methylated cytosines as a standard. The upper and lower limits were imposed at ±20% of the calculated distances. The δ torsion angles were estimated from the analysis of $^3J_{H1'-H2'}$ in ^{31}P decoupled DQF-COSY spectra. All χ torsion angles were constrained to $-120 \pm 90°$ (*anti*) based on intraresidual H6/8–H1′ NOEs from a 50 ms NOESY spectrum, except for *C1, which was constrained to $20 \pm 90°$ (*syn*). The following torsion angle restraints for residues *C1–G4 and *C9–G12 were used: (i) α and ζ were constrained to $0 \pm 120°$ excluding *trans* conformation since ^{31}P chemical shifts were within 1 p.p.m. range. MD calculations with unrestrained α and ζ torsion angles of stem residues converged to the same family of structures. The inclusion of these torsion angle restraints did not result in improvement in the quality of the structures of the stem region. (ii) β were constrained to $180 \pm 60°$ (*trans*) based on the low intensity of P-H5′/H5″ peaks in HP-COSY experiment. (iii) ε[C3′-C2′-O2′-P] were constrained to $240 \pm 50°$ excluding unfavorable *gauche*$^+$ conformation. None of the backbone torsion angles (α, β, γ, ε and ζ) was constrained for residues A5–*U8. No NOEs and torsion angle restraints were used for the MOE substituents. All the calculations were performed by using SANDER module of AMBER 6.0 software (19) and the Cornel *et al*. (20) force field. The Gaussian 98 program (21) was used to calculate HF/6-31G* electrostatic potential of modified residues, which was fitted by using RESP module of AMBER 6.0 to obtain partial atomic charges. The force field parameters for MOE group were used from the previous studies (22). Starting structures were prepared using up to 8 ps unrestrained molecular dynamics at elevated temperatures ranging from 600 to 4000 K. Structures were calculated in two stages. In the first stage, the calculations of 300 structures were performed *in vacuo* for 60 ps with a time step of 1 fs. The molecule was heated at 1000 K (31 ps),

then the temperature was gradually scaled down to 100 K (16 ps) and finally reduced to 0 K (3 ps). The family of 30 structures with the lowest total energies and the NMR restraint violation energies were then subjected to the second stage of restrained molecular dynamics using the Generalized Born implicit solvation model (23). Protocol involved a 20 ps restrained MD with heating at 800 K (8 ps), followed by the first cooling step to 100 K (10 ps) and the final cooling step to 0 K (2 ps). The force constants for distance and torsion angle restraints were 50 kcal mol^{-1} $Å^{-2}$ and 200 kcal mol^{-1} rad^{-2}, respectively. Weak base-planarity restraints for G2·*C11, *C3·G10 and G4·*C9 base pairs (25 kcal mol^{-1} rad^{-2}) were applied only in the first stage. The hydrogen bonds of these base pairs were maintained by distance restraints (24). The resulting structures were subjected to 1000 steps of conjugate gradient minimization using experimental restraints. The analyses of 30 final structures were carried out by using CARNAL and SUPPOSE programs of AMBER 6.0.

UV spectroscopy

Thermal melting experiments were collected on Beckman DU Series 600 spectrophotometer. Absorption was recorded as a function of temperature at 260 nm. Oligomer samples were prepared in the concentration range of 8–266 μM at various salt and pH conditions. The temperature was varied from 2 to 80°C and increased at a rate of 1.0°C min^{-1}. The molar extinction coefficient for 3′-MOE-2′,5′-RNA was estimated using the nearest-neighbor approximation for 3′,5′-linkages. Melting profiles were obtained by taking the first derivative of the absorbance with respect to temperature ($\delta A_{260}/\delta T$) where melting temperature (T_m) was the maximum of curve. Analysis of the melting profiles was performed by using ORIGIN software (OriginLab, Northhampton, MA).

Coordinate deposition

The coordinates for the 30 lowest energy structures of 3′-MOE-2′,5′-RNA hairpin have been deposited in the Protein Data Bank with accession codes 1XV6.

RESULTS AND DISCUSSION

UV and NMR melting studies

UV melting experiments on 3′-MOE-2′,5′-RNA in 1 M NaCl solution at pH 6.0 reveal two transitions (Figure 2a). The T_m of the higher temperature transition ($T_m = 48°C$) does not change as a function of oligomer concentration, whereas the low temperature transition shows a marked decrease in T_m from 23°C at 123 μM to 15°C at 8 μM. The concentration-independent T_m of 48°C corresponds to a monomolecular process, such as melting of a hairpin form of 3′-MOE-2′,5′-RNA. The low temperature transition, which exhibits concentration dependence of T_m, is in agreement with melting profile of a bimolecular form such as a duplex. Similar features of melting transitions are also observed at 1 M NaCl and pH 7.5, where hairpin melts at 45°C (Figure 2b). Analogously, UV melting experiments at 50 mM NaCl and pH values of 6.0 and 7.4 (Figure 2c and d) exhibit the main transition with higher T_m, whose broad melting profile overlaps with the minor transition with lower T_m. Several studies on analogous palindromic 3′,5′-linked Dickerson–Drew DNA dodecamer demonstrated

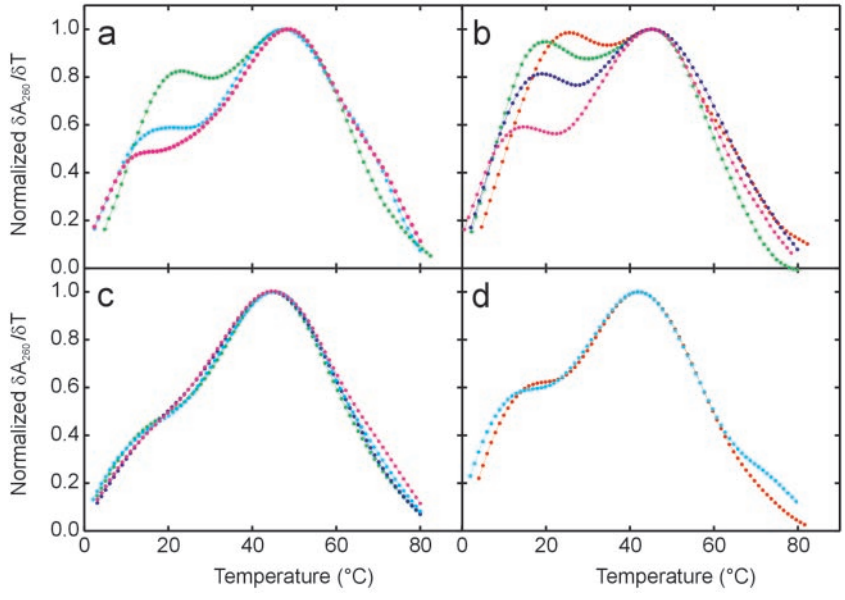

Figure 2. UV melting profiles of 3′-MOE-2′,5′-RNA at various oligomer and salt concentrations and pH. The calculated fits of the first derivatives of a melting curves are presented as a function of temperature at the following solution conditions: (**a**) 1 M NaCl and pH of 6.0 over a concentration range of 8 μM (magenta), 17 μM (cyan) and 123 μM (green). The T_m of high temperature transition is 48°C and low temperature transition is melted in the range of 15–23°C. (**b**) The 1 M NaCl and pH 7.5 over a concentration range of 9 μM (magenta), 39 μM (blue), 101 μM (green) and 266 μM (orange). The T_m of high temperature transition is 45°C, whereas the T_m of low temperature transition is in the range of 15–26°C. (**c**) The 50 mM NaCl and pH of 6.0. Concentrations are 9 μM (magenta), 23 μM (cyan), 39 μM (blue) and 169 μM (green). The T_m of high temperature transition form is 45°C whereas the T_m of low temperature transition appears under the broad transition profile of high temperature form. (**d**) The 50 mM NaCl and pH of 7.4. Concentrations are 17 μM (cyan) and 270 μM (orange). The T_m of high temperature transition is near 42°C and low temperature transition melts in 16–20°C range.

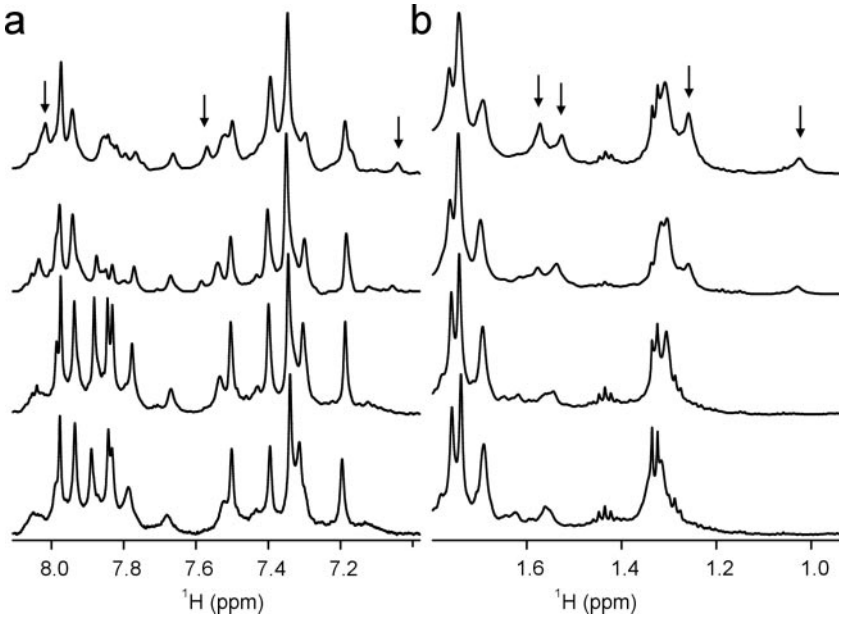

Figure 3. Comparison of (**a**) aromatic and (**b**) methyl region of ^{1}H NMR spectra of 3′-MOE-2′,5′-RNA at various strand concentrations (0.2, 0.4, 2.6 and 3.0 mM from bottom to top). Arrows indicate signals of the duplex that are separated from signals of the dominant hairpin form. Spectra were recorded in 100% ^2H_2O at 30°C, 50 mM NaCl and pH* 7.4.

that its melting transition curves at low salt concentration exhibited sharp duplex to hairpin transition, which was followed by a broad hairpin to denatured-strand transition at higher temperature (25,26). The self-complementary 3′,5′-DNA dodecamer with TA residues in the center of the sequence also formed hairpin intermediate during its melting transition at low salt concentrations, whereas only duplex to denatured-strand transition was observed at high salt concentrations (27). Our UV melting studies clearly ascertain that while at high salt conditions population of duplex form of 3′-MOE-2′,5′-RNA increases, the hairpin form is present nonetheless at both low and high salt concentrations.

A recent study on a fully 2′-MOE substituted 5′-CGCGAAUUCGCG-3′ RNA dodecamer has shown that it forms a stable duplex with T_m of over 82°C at 150 mM NaCl and pH 7.0 (28). Similarly, our preliminary UV melting studies on the analogous 2′-MOE-5′-*CG*CGAA*U*U*CG*CG^1-3′ RNA (where * denotes C5-methylation of C and U, and G^1 is 2′-deoxyguanosine) also show concentration-dependent melting transitions with very high T_m of over 90°C, which indicates the formation of a very stable duplex with strong base-pairing and stacking interactions. In contrast, the duplex form of 3′-MOE-2′,5′-RNA exhibits significantly lower T_m in comparison with 3′,5′-linked RNA and thus clearly shows that the chemical nature of phosphodiester linkage and other sugar substituents have a profound effect on the stability of their duplex structures. Furthermore, the duplex represents at UV concentration range only a minor secondary structure of 3′-MOE-2′,5′-RNA in solution.

We then acquired 1D ^{1}H NMR spectra at various temperatures and oligomer concentrations that were both found to control hairpin ↔ duplex equilibrium of 3′-MOE-2′,5′-RNA. The simultaneous presence of both forms leads to spectral overlap and line width broadening of proton resonances. Nevertheless, analysis of NMR data clearly shows that the relative amount of duplex form increases by the lowering of sample temperature, or with the increase in oligomer concentration (Figure 3).

At 0.9 mM strand concentration, 50 mM NaCl and 0°C, the relative populations of hairpin and duplex forms are equal and involved in slow exchange on the NMR timescale. As temperature is increased to 30°C the hairpin becomes predominant, whereas the duplex is undergoing melting transition. On the other hand, proton NMR spectra at 9.0 mM strand concentration and 0°C show that the equilibrium is completely shifted to duplex form. Only a minor amount of hairpin (33%) is present at this concentration at 30°C. Further increase in temperature above 35°C at both 0.9 and 9.0 mM strand concentrations, initiates the melting of the hairpin, which is in agreement with the broad UV melting profiles for hairpin to denatured state transition. The proton spectra at 9.0 mM strand concentration above 60°C show that hairpin and denatured forms are still in slow exchange on the NMR timescale.

The intensity of well resolved *U8 C7(H7)$_3$ resonance of hairpin was measured and compared with the corresponding intensities of *U8 C7(H7)$_3$ and *C9 C7(H7)$_3$ of duplex in order to determine the equilibrium constants. The equilibrium constants determined in the temperature range from 0 to 40°C were then used to calculate thermodynamic parameters for the duplex to hairpin transition. The van't Hoff analysis assuming a two-state duplex-hairpin transition afforded an estimate of enthalpy (ΔH) and entropy (ΔS) of interconversion, which were 17 ± 1 kcal mol^{-1} and 45 ± 3 cal mol^{-1} K^{-1}, respectively. On the other hand, direct fitting of differential UV melting curves with the use of the van't Hoff relationship (29–31) afforded ΔH of 21 ± 1 kcal mol^{-1} for hairpin to denatured-state transition at 50 mM NaCl and pH 6.0.

NMR spectroscopy of 3′-MOE-2′,5′-RNA

Our initial UV and NMR measurements have shown that 3′-MOE-2′,5′-RNA adopts both hairpin and duplex structures. Their imino proton resonances shown in Figure 1b were assigned in water NOESY spectra at 9.0 mM strand concentration at 5 and 25°C using well-established methods (32). The observation of only one set of NOEs for the duplex of 3′-MOE-2′,5′-RNA affirms its symmetric palindromic nature. The G2 H1 of the duplex shows NOE cross-peaks with the two *C11 amino protons (hydrogen bonded and non-bonded), which indicates the formation of a Watson–Crick G2·*C11 base pair. The G2 H1 also shows NOE contact across strand to G10 H1 of the duplex. G4 H1 and G10 H1 of the duplex show NOEs to *C9 and *C3 amino protons, respectively. Furthermore, two strong NOEs of the duplex are observed correlating G2 H1 and G10 H1 to *C11 C7(H7)$_3$ and *C3 C7(H7)$_3$, respectively, while weak NOE correlates G4 H1 and *C9 C7(H7)$_3$. Strong A5 H2–*U8 H3 and A6 H2–*U7 H3 NOEs indicate the formation of respective Watson–Crick base pairs. The predominant form at 9.0 mM strand concentration is duplex, while hairpin is present at higher temperature (25°C). Interestingly, weak NOE between A5 H2 and *U8 H3 indicating the formation of Watson–Crick A5·*U8 base pair is detected for the hairpin form at 25°C. However, this restraint was not used in the structure calculations (*vide infra*). No other imino proton NOE connectivity for hairpin is obtained at 9.0 mM strand concentration.

The imino proton spectra collected at 0.9 mM strand concentration, pH 7.4 and 20°C, where hairpin predominates, show low signal-to-noise ratio and severe line width broadening in the region characteristic for Watson–Crick A·*U and G·*C base pairs that hampered their assignments. As ROESY data show no changes in chemical shifts of aromatic and methyl protons for the ends of the sequence (residues *C1–G4, G10–G12), while changes are observed for the central part (residues A5–*C9), we assumed that imino proton resonances of residues at the ends of the sequence are isochronous for hairpin and duplex forms. Consequently, very weak Watson–Crick hydrogen bond distance and planarity restraints for G2·*C11, *C3·G10 and G4·*C9 base pairs in the stem of the hairpin were applied in structure calculations. ^{1}H spectrum obtained at 0.9 mM strand concentration, 50 mM NaCl, pH 6.8 (cacodylic buffer) and 0°C shows a resonance at 11.18 p.p.m., which is in the region of imino proton resonances associated with unpaired or partially unstacked residues (16) and corresponds to *U7 H3 of hairpin. In support of unstacked conformation of *U7, NOESY data show no cross-peaks correlating *U7 H3 with other protons. No slowly exchanging imino resonances are observed for the terminal *C1·G12 at both 0.9 and 9.0 mM concentration due to fraying ends.

The simultaneous presence of hairpin and duplex structures makes NMR structural studies sometimes problematic, since the structural features that set these species apart from one another, tend to have similar NOE patterns and do not provide a reliable basis for structure determination. Consequently, low oligomer (0.9 mM) and salt concentrations (50 mM NaCl) were used where hairpin is greatly predominant (>90% at 30°C and pH* 7.4). The standard protocols for resonance assignment using DQF-COSY, TOCSY and NOESY experiments were applied. Sequential base H8/6–sugar H1′

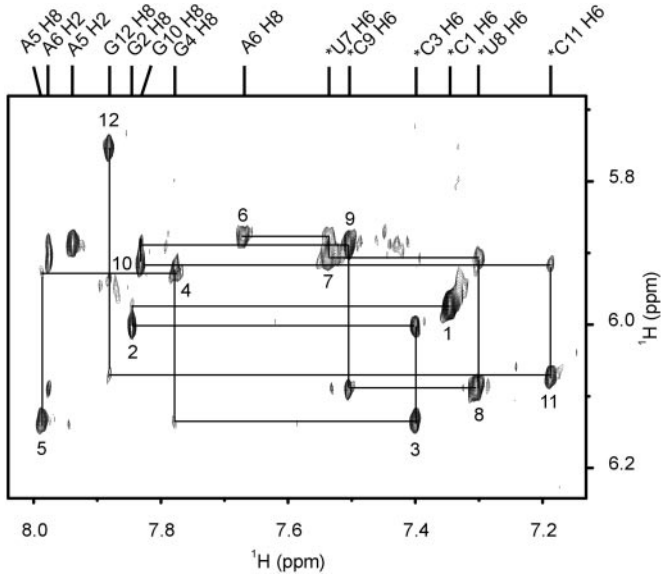

Figure 4. The aromatic–anomeric region of NOESY spectrum (200 ms mixing time) recorded at 30°C in 100% ^2H_2O. Sample conditions were 0.9 mM strand concentration, 50 mM NaCl and pH* 7.4. Sequential walk is indicated.

connectivities in the 200 ms NOESY spectrum at 30°C can be traced throughout the stem region, which is consistent with the formation of a right-handed helix (Figure 4). The following additional sequential NOE cross-peaks are detected: G2 H8 to *C3 C7(H7)$_3$, *U8 H6 to *C9 C7(H7)$_3$ and G10 H8 to *C11 C7(H7)$_3$. At 50 ms mixing time an intense intraresidual NOE is observed between *C1 H6 and its H1′, which is comparable in intensity with the pyrimidine C7(H7)$_3$–H6 cross-peak and thus indicates that terminal *C1 adopts predominantly *syn* conformation. In full support, weak NOEs from *C1 C7(H7)$_3$ to both G2 H1′ and G12 H1′ are observed. Terminal residues of DNA as well as RNA oligonucleotides with 2′,5′-linkages seem to prefer *syn* conformation (9,33). Intranucleotide H6/8–H1′ NOEs of all other residues are weak and only observed at longer mixing times as expected for nucleotides with *anti* conformation across glycosidic bonds. The methyl proton resonances of the 3′-MOE groups do not exhibit resolved NOEs to other protons.

The sequential aromatic H8/6–anomeric H1′ NOE connectivity network of the hairpin is broken at A5–A6 step, whereas it can be followed in the rest of the loop and stem regions. The presence of strong cross-strand A5 H2 to *C9 H1′ NOE suggests that A5 is incorporated in the loop and it is possibly involved in hydrogen bonding with cross-strand *U8. This type of strong NOE interaction has been observed in A-form helix geometry of 3′,5′-RNA where H2 of adenosine is near the center of the base pair, as opposed to the other aromatic and sugar protons, which are situated on the perimeter (12). No NOE between A5 H2 and A6 H1′ can be unambiguously assigned, but is presumed to overlap with intense and broad A5 H2–*C9 H1′ NOE cross-peak due to the negligible chemical shift difference of A6 H1′ and *C9 H1′. No distance restraint was applied for A5 H2 and A6 H1′ protons. A6 H2 shows cross-strand NOEs to *U8 H1′, *U8 H6 and *U8 C7(H7)$_3$, which indicate that A6 base is

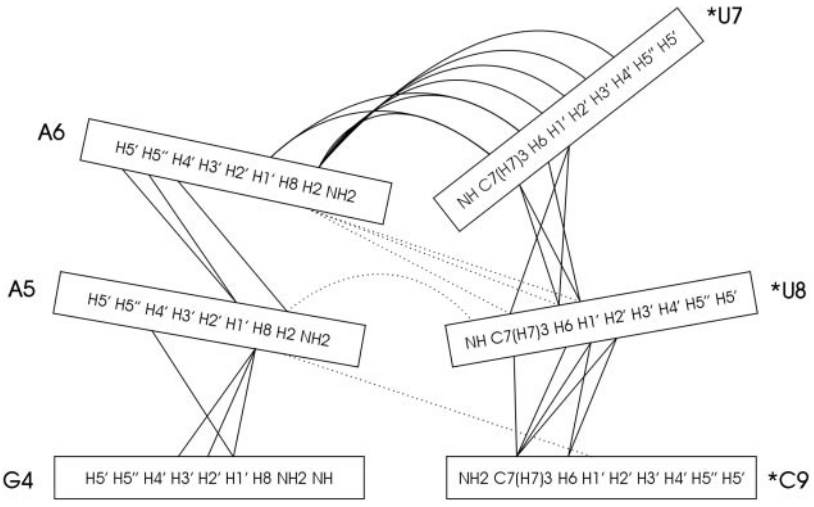

Figure 5. Overview of the interresidual NOEs in the 2′,5′-RNA hairpin loop. Sequential and long-range NOE connectivities are shown by solid and dotted lines, respectively.

oriented towards *U8. Furthermore, A6 H2 displays NOEs to H6, C7(H7)$_3$, H1′, H2′ and H3′ of *U7 that require the proximity of A6 H2 and sugar ring of *U7 as well as they define orientation of aromatic ring of *U7. The *U7 C7(H7)$_3$ protons show NOE contact to A6 H1′ and unusually intense 'forwards' NOE to *U8 H1′. The numerous NOEs among residues A5, A6, *U7, *U8 and *C9 demonstrate that the conformation of loop is well defined (Figure 5).

The analysis of DQF-COSY data at 30°C shows that A5 and G12 exhibit *S*-type sugar conformation, whereas the absence of cross-peaks in H1′–H2′ region for A6 and *U7 as well as *C9 suggests that their sugar rings exist predominantly in *N*-type conformations. The $^3J_{H1'-H2'}$ coupling constants of all other residues lie in the intermediate range from 3 to 6 Hz, which indicates that the equilibrium between *N*-type and *S*-type sugar conformations in 3′-MOE-2′,5′-RNA is not driven to a particular conformation by the exocyclic groups on the sugar rings and in particular by 2′-phosphodiester functionality (34,35). On the other hand, Premraj *et al*. (33) have shown that 2′,5′-RNA forms A-type duplex with *S*-type sugar conformations. Introduction of 3′-MOE group in trimers and tetramers leads to the stabilization, but not a complete shift of $N \leftrightarrow S$ equilibrium to *N*-type sugar conformation (35). In this respect, DQF-COSY data show that the majority of stem sugar rings in 3′-MOE-2′,5′-RNA are involved in an unbiased $N \leftrightarrow S$ pseudorotational equilibrium. More quantitative data are needed to establish correlations between tuning of $N \leftrightarrow S$ equilibrium and drive of duplex–hairpin equilibrium by 3′-MOE group in 2′,5′-RNA. Although functional groups influence predisposition of a particular nucleotide to adopt certain conformation, they are not the only factors that determine the folding process of oligonucleotide.

Solution structure of 3′-MOE-2′,5′-RNA hairpin

Structures were calculated with a molecular dynamics/simulated annealing protocol using mostly NOE distance restraints of non-exchangeable protons. High number of NOE distance restraints for residues of the loop demonstrates that hairpin loop adopts a well-defined structure (Figure 6a).

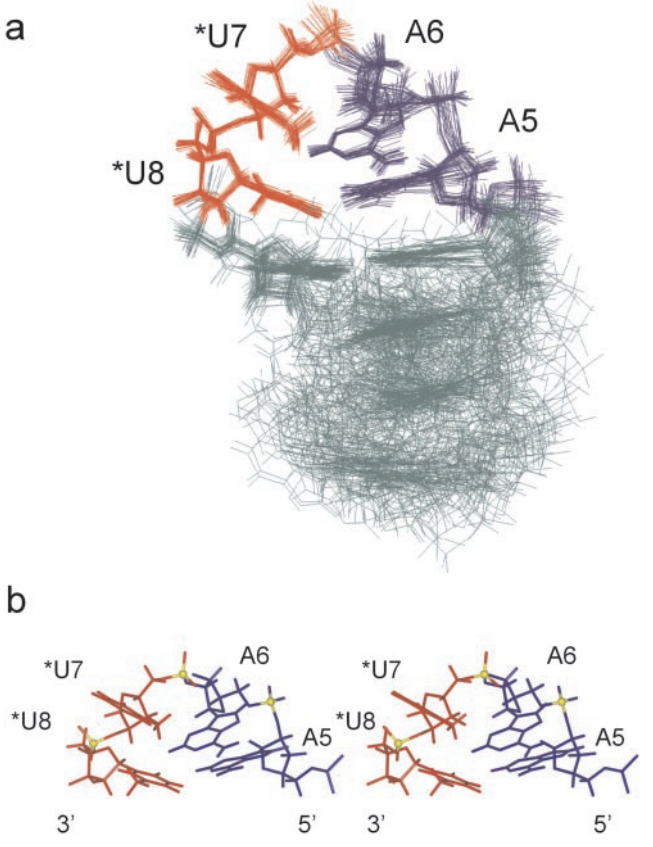

Figure 6. Solution structure of 3′-MOE-2′,5′-RNA hairpin. (**a**) Superposition of the 30 final structures based on the loop residues A5–*U8. The heavy atoms without MOE groups have been superimposed. The loop residues are colored blue (A) and red (*U). Stem residues are coloured green. (**b**) Stereoview of a single representative structure of the 2′,5′-linked RNA hairpin loop. All atoms without MOE groups are displayed.

The ensemble of 30 final structures with superimposed heavy atoms of the loop residues A5–*U8 exhibits a pairwise r.m.s.d. value of 0.65 Å for the loop residues (Table 1). On the other hand, the lower number of NOE restraints

Table 1. Structural statistics for 3′-MOE-2′,5′-RNA hairpin

Experimental data used for structure calculations	
NOE-derived distance restraints	
Intranucleotide NOEs	92
Internucleotide NOEs	54
Hydrogen bond for paired residues	15
Torsion angle restraints	49
NOE violations (Å)	0 > 0.4
Angle violations (°)	0 > 6
Deviations from idealized covalent geometry	
Bonds (Å)	0.0098 ± 0.0003
Angles (°)	2.77 ± 0.09
Heavy atom r.m.s.d. (Å)[a]	
Residues A5–*U8	0.65
Residues *C1–G4, *C9–G12	1.32

[a]Final 30 structures were used to calculate the pairwise Cartesian coordinate r.m.s.d.

for the stem region (residues *C1–G4 and *C9–G12) is reflected in the r.m.s.d. of 1.32 Å when superposition of heavy atoms was based on the stem residues. In this respect, DQF-COSY data show that the majority of stem sugar rings are involved in an unbiased $N \leftrightarrow S$ pseudorotational equilibrium, which is consistent with the greater flexibility of the stem region. Analysis of the final structures shows the following conformational preferences of MOE groups: (i) *gauche*$^-$ and *trans* rotamers are greatly preferred along C3′–O3′ bonds, (ii) torsion angles [C3′-O3′-CA-CB] are predominantly in *trans* conformation, (iii) fragments [O3′-CA-CB-O] adopt *gauche*$^+$ and *gauche*$^-$ conformations. It should be noted, however, that no restraints for 3′-MOE groups were included in the structure calculations owing to the absence of resolved NOEs.

Perusal of structures shown in Figure 6a demonstrates that residues A5 and *U8 are partially stacked on the nearby G4·*C9 and are predisposed to the formation of Watson–Crick base pair. G4pA5 step does not exhibit characteristics of A-form helix, e.g. G4 adopts *N*-type, while A5 adopts *S*-type sugar conformation. In addition, intrastrand P–P distance is 7.6 Å, which is well over 5.9 Å found in A-type helix. Experimentally observed NOE contacts for G4pA5 step are not characteristic for A-type helix. The loop residues A6 and *U7 are unpaired and adopt *N*-type sugar ring conformation. The aromatic ring of *U7 is oriented towards the minor groove, whereas A6 is located in the major groove. A6 is only partially stacked on pyrimidine moiety of A5 and is slightly bulged out from the core of the loop (Figure 6b). The spatial positions of O4′ atoms of A6 and *U8 and their lone-pair electrons imply stabilization through an $n \rightarrow \pi^*$ interactions with aromatic rings of A5 and *U7, respectively. Such stabilizing stacking interactions have been described in several nucleic acid structures (36,37) and, particularly, in 2′,5′-linked nucleotides (2).

The orientation across glycosidic bond of *U7 is in the high *anti* range (Figure 6b). Intraresidual C7(H7)$_3$–H6 NOESY cross-peak of *U7 as well as respective signal in DQF-COSY spectrum are severely broadened, which suggests that the *U7 might be involved in a dynamic motion on a millisecond time-scale. Although loop residues adopt a rather compact and well defined structure they exhibit some degree of flexibility.

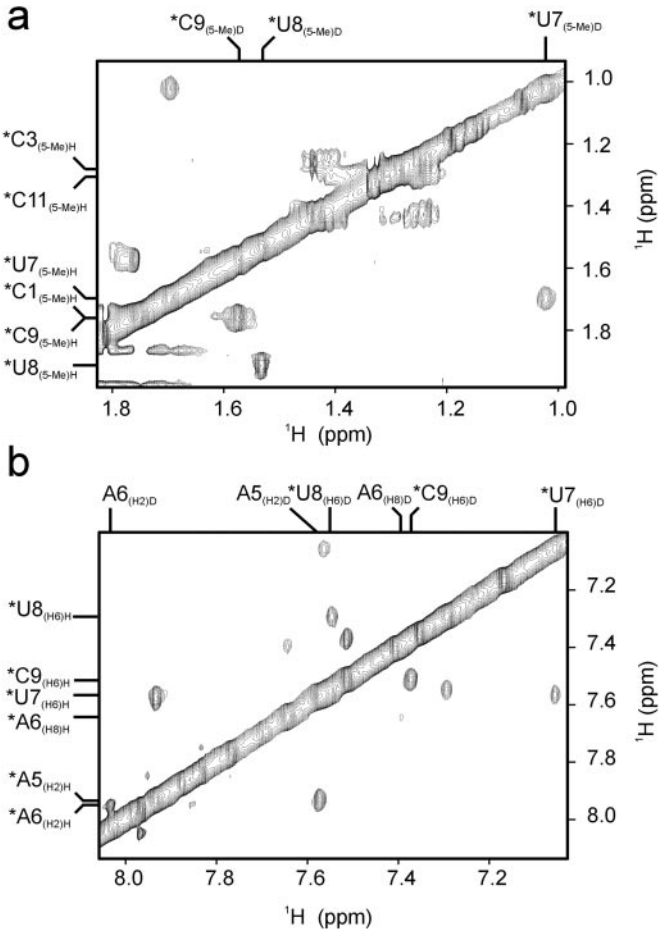

Figure 7. (**a**) Methyl–methyl and (**b**) aromatic–aromatic region of ROESY spectrum (100 ms mixing time) recorded at 25°C in 100% ^2H_2O. The assignments of the resolved exchange signals for hairpin (H) and duplex (D) forms are indicated. Sample conditions were 3.0 mM strand concentration, 350 mM NaCl and pH* 7.4.

Conformational exchange

Unusually strong cross-peaks in methyl–methyl and aromatic–aromatic region of NOESY spectra at 3.0 mM strand concentration suggest an exchange between hairpin and duplex, which has been confirmed by using ROESY experiments (Figure 7). The positive off-diagonal exchange cross-peaks are observed for protons of the loop residues [*U7 C7(H7)$_3$, *U8 C7(H7)$_3$, A5 H2, A6 H8, A6 H2, *U7 H6 and *U8 H6] and nearby stem residue [*C9 C7(H7)$_3$ and *C9 H6]. The largest differences in chemical shifts of aromatic and methyl protons for hairpin and duplex are found for the central residues of the sequence (Table 2). The largest upfield chemical shift changes upon moving from hairpin to duplex are observed for *U7 H6 and *U7 C7(H7)$_3$. A possible explanation for the observed chemical shift differences is found in the structural features of the duplex form, where *U7 is base paired with A6 and stacked on the preceding A6·*U7, where they experience their ring current effects. In hairpin, *U7 is unstacked and points out of the loop. The upfield shift of A5 H2 in the duplex can also be interpreted by the ring current effect of the stacked A6. No changes in chemical shifts of G4 are observed for hairpin and duplex

Table 2. Chemical shifts (p.p.m.) of assigned resonances for hairpin and duplex form of 3′-MOE-2′,5′ RNA[a]

Aromatic protons		Difference	Methyl protons		Difference
A5 H2	7.93	0.36	*U7 C7(H7)$_3$	1.70	0.67
	7.57			1.03	
A6 H2	7.96	−0.13	*U8 C7(H7)$_3$	1.92	−0.39
	8.03			1.53	
A6 H8	7.64	0.24	*C9 C7(H7)$_3$	1.76	0.18
	7.40			1.58	
*U7 H6	7.56	0.50			
	7.06				
*U8 H6	7.30	−0.24			
	7.54				
*C9 H6	7.51	0.14			
	7.37				

[a]The top value for each proton corresponds to chemical shift of hairpin, while chemical shift of duplex is shown below. The chemical shift difference is calculated as δ(hairpin) − δ(duplex).

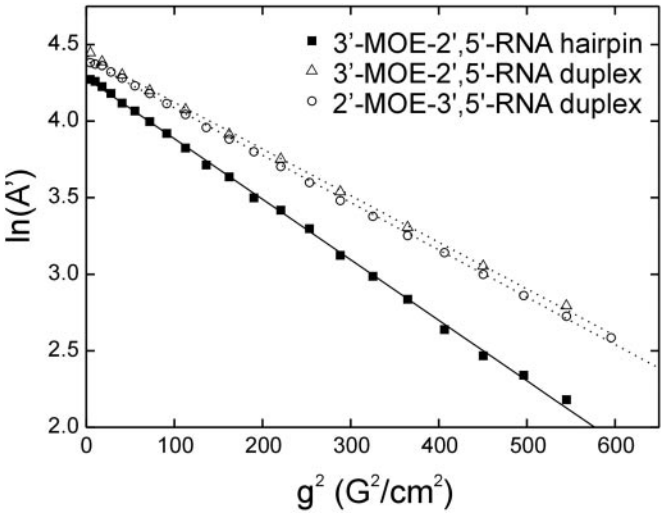

Figure 8. ^{1}H NMR signal intensity [ln(A')] as a function of gradient field strength (g^2) at 25°C. The filled squares represent A6 H2 signal intensity of 3′-MOE-2′,5′-RNA hairpin, while the open triangles represent A6 H2 of the duplex form. The open circles represent the average signal intensity of aromatic resonances of 2′-MOE-3′,5′ RNA duplex. The sample conditions were 3.0 mM strand concentration, 350 mM NaCl and pH* 7.4 in 100% ^2H_2O.

forms, which suggest that stacking pattern of A5 on G4 is conserved in both structures. On the other hand, protons of *C9 experience changes in chemical shifts, although NOEs between *U8 and *C9 protons suggest similar stacking interactions in both secondary structures.

Determination of translational diffusion constants (D_T) by using PFG NMR spectroscopy provides a powerful tool to evaluate the secondary structures of nucleic acids (38,39). The D_T values of 3′-MOE-2′,5′-RNA hairpin and duplex structures were measured and compared with a reference 12mer 2′-MOE-3′,5′-RNA duplex of identical sequence (Figure 8). The ratio between D_T of the hairpin and duplex forms of 3′-MOE-2′,5′-RNA is 1.30, which is comparable with the reported $D_{monomer}$:D_{dimer} ratio for RNA oligomers (38). The highest degree of agreement of slopes of lines that correspond to duplex forms of modified 2′,5′- and 3′,5′-linked RNA dodecamers offers experimental support for the similarity of their secondary structures (Figure 8).

pH-dependent structural equilibrium of 3′-MOE-2′,5′-RNA

The aromatic proton resonances are relatively sharp at 0.9 mM strand concentration, pH 7.4 and 20°C, which is in accordance with the prevalence of the hairpin form. New set of resonances, corresponding to duplex form appear upon lowering of pH to 6.6 (Figure 9). Unfortunately, the line width broadening hampered our attempt to plot individual chemical shifts as a function of pH in order to construct titration curves. The perusal of methyl region of 1D NMR proton spectra at 0.9 mM strand concentration shows that change in pH from 7.4 to 6.6 at 20°C results in a significant increase in the relative amount of duplex (Figure 9b). As expected, the population of duplex is also increased upon lowering of sample temperature from 20 to 5°C at both pH 7.4 and 6.6. Similar pH-dependent dimerization has been observed earlier for DNA oligomer forming hairpin and duplex structures (40).

Several relatively sharp imino proton resonances are observed at 0.9 mM strand concentration, pH 7.4 and 5°C (Figure 9a). Almost all imino proton resonances severely broaden upon decreasing pH to 6.6 while no changes in chemical shifts are observed. Similar line width broadening of imino proton resonances occurs by lowering pH at 20°C. Imino protons are exchanged with the bulk water, which contributes to the line widths of imino proton resonances. However, the observed line width broadening is opposite to what would be expected if the increase of the line widths was a result of an increase in the rate of exchange with bulk water (41). The broadening of the imino proton resonances at 0.9 mM strand concentration by lowering pH can be attributed to exchange between hairpin and duplex structures, since lowering of pH increases duplex population. Such unusual pH dependence of the line width broadening of imino proton resonances was also observed in a hairpin loop of a nucleolin recognition element construct (42) and in the HIV-1 dimerization initiation site kissing complex (43).

We also examined the effect of pH changes at 9.0 mM strand concentration and 5°C, where only duplex was observed. As it is the case at 0.9 mM strand concentration, the line widths of the imino proton resonances show profound pH dependences with relatively sharp lines observed at higher pH and exchange broadening at lower pH (Figure 10a). The effect is most pronounced for G4 and G10, which are involved in Watson–Crick base pairs. Only small broadening of imino proton resonances of G2, *U7 and *U8 is observed. It is noteworthy that NOESY data show no indication of hairpin formation at 5°C and, therefore, the observed broadening cannot be attributed to exchange between hairpin and duplex structures. In full support, no changes are observed for non-exchangeable protons upon lowering of pH. Since broadening of imino resonances cannot be attributed to the exchange between hairpin and duplex structures we propose a dynamic, 'breathing' model where the interstrand hydrogen bonds are formed and disrupted at the rate that is intermediate on the NMR timescale. Such base pair dynamics is pH-dependent and explains why imino protons are broadened, while non-exchangeable proton resonances remain relatively sharp due

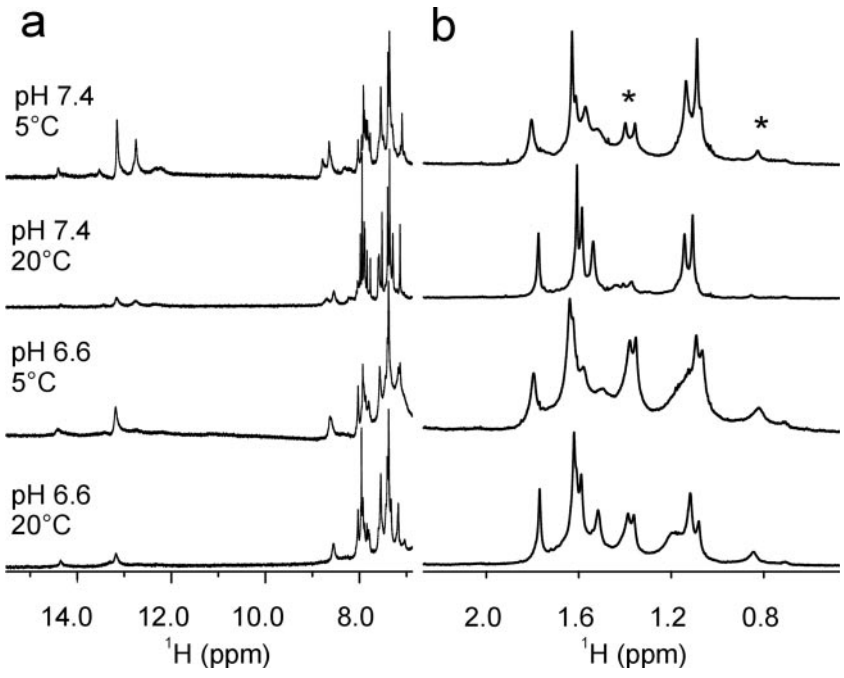

Figure 9. ^{1}H NMR spectra of (**a**) imino and aromatic proton region and (**b**) methyl proton region of 3′-MOE-2′,5′-RNA as a function of pH and temperature. The vertical scale of imino and aromatic region is doubled. The sample was 0.9 mM strand concentration, 50 mM NaCl in 90% H_2O/10% $^{2}H_2O$. Stars indicate $C7(H7)_3$ resonances of duplex form whose intensities increase upon lowering pH and temperature.

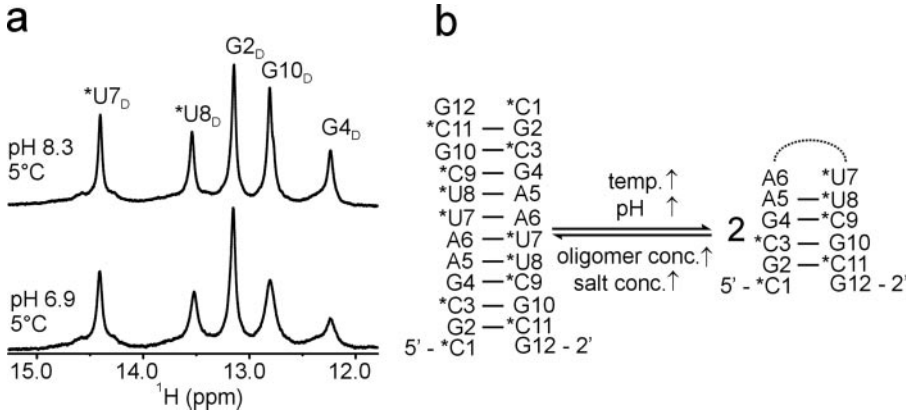

Figure 10. (**a**) Imino proton spectra of 3′-MOE-2′,5-RNA at 5°C as a function of pH. The sample was 9 mM strand concentration, 50 mM NaCl in 90% H_2O/10% $^{2}H_2O$. Imino protons involved in Watson–Crick base pairs of duplex (D) are shown. (**b**) Schematic representation of the duplex–hairpin equilibrium of 3′-MOE-2′,5-RNA. Closed lines represent Watson–Crick base pairs.

to small hydrogen bonding contributions to the chemical shift of non-exchangeable protons. In conclusion, lowering of pH plays a dual role that on one hand drives hairpin ↔ duplex equilibrium toward duplex structures, and on the other influences dynamics of opening and closing of base pairs, at the same time.

CONCLUSION

NMR and UV spectroscopic studies have demonstrated that 3′-MOE-2′,5′-RNA is involved in an equilibrium between hairpin and duplex structures, which is driven by oligomer and salt concentrations as well as pH (Figure 10b). Lowering of pH drives equilibrium toward duplex. Unusual effect of pH is observed for imino proton resonances that show strong pH dependences over a narrow physiological range with the exchange broadening observed at lower pH and relatively sharp lines observed at higher pH. NMR structure of 3′-MOE-2′,5′-RNA hairpin displays a unique and well-defined loop that is stabilized by Watson–Crick A5·*U8 base pair inside the loop and by $n \rightarrow \pi^*$ stacking interactions of O4′ lone-pair electrons of A6 and *U8 with the aromatic rings of A5 and *U7, respectively. The solution structure of the modified 2′,5′-linked RNA hairpin provides an important model in the field of modified nucleic acids where the structural data are still scarce. It has been demonstrated that 2′,5′-linked RNA are significantly more resistant toward nuclease

degradation in comparison with their 3′,5′-linked analogs. Recent study showed that the 2′,5′-linked RNA loop structure is recognized by HIV-1 reverse transcriptase and acts as a potent inhibitor of RNase H activity of HIV-1 RT when present within the appropriate hairpin stem (44). New structural data contribute to the repertoire of novel RNA structural motifs that assists in the design of new 2′,5′-linked RNA aptamers and ribozymes.

ACKNOWLEDGEMENTS

We thank Dr M. Manoharan and Isis Pharmaceuticals Inc. for the oligonucleotide. We acknowledge the Ministry of Higher Education, Science and Technology of the Republic of Slovenia (grant nos P1-0242-0104 and J1-6140-0104) and European Commission (contract no. ICA1-CT-2000-70034) for their financial support. Funding to pay the Open Access publication charges for this article was provided by National Institute of Chemistry, Slovenia.

Conflict of interest statement. None declared.

REFERENCES

1. Usher,D.A. and McHale,A.H. (1976) Hydrolytic stability of helical RNA: a selective advantage for the natural 3′,5′-bond. *Proc. Natl Acad. Sci. USA*, **73**, 1149–1153.
2. Parthasarathy,R., Malik,M. and Fridey,S.M. (1982) X-ray structure of a dinucleoside monophosphate A2′p5′C that contains a 2′–5′ link found in (2′–5′)oligo(A)s induced by interferons: single-stranded helical conformation of 2′–5′-linked oligonucleotides. *Proc. Natl Acad. Sci. USA*, **79**, 7292–7296.
3. Srinivasan,A.R. and Olson,W.K. (1986) Conformational studies of (2′–5′) polynucleotides: theoretical computations of energy, base morphology, helical structure and duplex formation. *Nucleic Acids Res.*, **14**, 5461–5497.
4. Dougherty,J.P., Rizzo,C.J. and Breslow,R. (1992) Oligodeoxynucleotides that contain 2′,5″ linkages: synthesis and hybridization properties. *J. Am. Chem. Soc.*, **114**, 6254–6255.
5. Hashimoto,H. and Switzer,C. (1992) Self-association of 2′,5′-linked deoxynucleotides: meta-DNA. *J. Am. Chem. Soc.*, **114**, 6255–6256.
6. Kierzek,R., He,L.Y. and Turner,D.H. (1992) Association of 2′–5′ oligoribonucleotides. *Nucleic Acids Res.*, **20**, 1685–1690.
7. Breslow,R. and Xu,R. (1993) Recognition and catalysis in nucleic acid chemistry. *Proc. Natl Acad. Sci. USA*, **90**, 1201–1207.
8. Jin,R.Z., Chapman,W.H., Srinivasan,A.R., Olson,W.K., Breslow,R. and Breslauer,K.J. (1993) Comparative spectroscopic, calorimetric, and computational studies of nucleic acid complexes with 2′,5″- versus 3′, 5″-phosphodiester linkages. *Proc. Natl Acad. Sci. USA*, **90**, 10568–10572.
9. Robinson,H., Jung,K.E., Switzer,C. and Wang,A.H.J. (1995) DNA with 2′–5′ phosphodiester bonds forms a duplex structure in the A-type conformation. *J. Am. Chem. Soc.*, **117**, 837–838.
10. Drew,H.R., Wing,R.M., Takano,T., Broka,C., Tanaka,S., Itakura,K. and Dickerson,R.E. (1981) Structure of a B-DNA dodecamer: conformation and dynamics. *Proc. Natl Acad. Sci. USA*, **78**, 2179–2183.
11. Dickerson,R.E., Drew,H.R., Conner,B.N., Wing,R.M., Fratini,A.V. and Kopka,M.L. (1982) The anatomy of A-DNA, B-DNA, and Z-DNA. *Science*, **216**, 475–485.
12. Chou,S.H., Flynn,P. and Reid,B. (1989) Solid-phase synthesis and high-resolution NMR studies of two synthetic double-helical RNA dodecamers: r(CGCGAAUUCGCG) and r(CGCGUAUACGCG). *Biochemistry*, **28**, 2422–2435.
13. Moore,P.B. (1999) Structural motifs in RNA. *Annu. Rev. Biochem.*, **68**, 287–300.
14. Hannoush,R.N. and Damha,M.J. (2001) Remarkable stability of hairpins containing 2′,5′-linked RNA loops. *J. Am. Chem. Soc.*, **123**, 12368–12374.
15. Denisov,A.Y., Hannoush,R.N., Gehring,K. and Damha,M.J. (2003) A novel RNA motif based on the structure of unusually stable 2′,5′-linked r(UUCG) loops. *J. Am. Chem. Soc.*, **125**, 11525–11531.
16. Varani,G., Aboul-ela,F. and Allain,F.H.-T. (1996) NMR investigation of RNA structure. *Prog. Nucl. Magn. Reson. Spectrosc.*, **29**, 51–127.
17. Stejskal,E.O. and Tanner,J.E. (1965) Spin diffusion measurements: spin echoes in the presence of a time-dependent field gradient. *J. Chem. Phys.*, **42**, 288–292.
18. Wu,D.H., Chen,A. and Johnson,C.S. (1995) Flow imaging by means of 1D Pulsed-Field-Gradient NMR with application to electroosmotic flow. *J. Magn. Reson. Ser. A*, **115**, 123–126.
19. Pearlman,D.A., Case,D.A., Caldwell,J.W., Ross,W.S., Cheatham,T.E., Debolt,S., Ferguson,D., Seibel,G. and Kollman,P. (1995) AMBER, a package of computer programs for applying molecular mechanics, normal mode analysis, molecular dynamics and free energy calculations to simulate the structural and energetic properties of molecules. *Comput. Phys. Commun.*, **91**, 1–41.
20. Cornell,W.D., Cieplak,P., Bayly,C.I., Gould,I.R., Merz,K.M., Ferguson,D.M., Spellmeyer,D.C., Fox,T., Caldwell,J.W. and Kollman,P.A. (1995) A second generation force field for the simulation of proteins, nucleic acids and organic molecules. *J. Am. Chem. Soc.*, **117**, 5179–5197.
21. Frisch,M.J., Trucks,G.W., Schlegel,H.B., Scuseria,G.E., Robb,M.A., Cheeseman,J.R., Zakrzewski,V.G., Montgomery,J.A., Stratmann,R.E., Burant,J.C. *et al.* (1998) Gaussian 98, Revision A.5 edn. Gaussian Inc., Pittsburgh, PA.
22. Lind,K.E., Mohan,V., Manoharan,M. and Ferguson,D.M. (1998) Structural characteristics of 2′-*O*-(2-methoxyethyl)-modified nucleic acids from molecular dynamics simulations. *Nucleic Acids Res.*, **26**, 3694–3699.
23. Tsui,V. and Case,D.A. (2000) Molecular dynamics simulations of nucleic acids with a generalized born solvation model. *J. Am. Chem. Soc.*, **122**, 2489–2498.
24. Saenger,W. (1984) *Principles of Nucleic Acid Structure*. Springer-Verlag, New York, NY.
25. Patel,D.J., Kozlowski,S.A., Marky,L.A., Broka,C., Rice,J.A., Itakura,K. and Breslauer,K.J. (1982) Premelting and melting transitions in the d(CGCGAATTCGCG) self complementary duplex in solution. *Biochemistry*, **21**, 428–436.
26. Marky,L.A., Blumenfeld,K.S., Kozlowski,S. and Breslauer,K.J. (1983) Salt dependent conformational transitions in the self-complementary deoxydodecanucleotide d(CGCAATTCGCG): evidence for hairpin formation. *Biopolymers*, **22**, 1247–1257.
27. Wemmer,D.E., Chou,S.H., Hare,D.R. and Reid,B.R. (1985) Duplex-hairpin transitions in DNA: NMR studies on CGCGTATACGCG. *Nucleic Acids Res.*, **13**, 3755–3772.
28. Teplova,M., Minasov,G., Tereshko,V., Inamati,G.B., Cook,P.D., Manoharan,M. and Egli,M. (1999) Crystal structure and improved antisense properties of 2′-*O*-(2-methoxyethyl)-RNA. *Nature Struct. Biol.*, **6**, 535–539.
29. Gralla,J. and Crothers,D.M. (1973) Free energy of imperfect nucleic acid helices. *J. Mol. Biol.*, **78**, 301–319.
30. Marky,L.A. and Breslauer,K.J. (1987) Calculating thermodynamic data for transitions of any molecularity from equilibrium melting curves. *Biopolymers*, **26**, 1601–1620.
31. John,D.M. and Weeks,K.M. (2000) van't Hoff enthalpies without baselines. *Protein Sci.*, **9**, 1416–1419.
32. Wijmenga,S.S. and van Buuren,B.N.M. (1998) The use of NMR methods for conformational studies of nucleic acids. *Prog. Nucl. Magn. Reson. Spectrosc.*, **32**, 287–387.
33. Premraj,B.J., Patel,P.K., Kandimalla,E.R., Agrawal,S., Hosur,R.V. and Yathindra,N. (2001) NMR structure of a 2′,5′ RNA favors A type duplex with compact C2′ endo nucleotide repeat. *Biochem. Biophys. Res. Commun.*, **283**, 537–543.
34. Plavec,J., Tong,W. and Chattopadhyaya,J. (1993) How do the gauche and anomeric effects drive the pseudorotational equilibrium of the pentofuranose moiety of nucleosides? *J. Am. Chem. Soc.*, **115**, 9734–9746.
35. Polak,M., Manoharan,M., Inamati,G.B. and Plavec,J. (2003) Tuning of conformational preorganization in model 2′,5′- and 3′,5′-linked oligonucleotides by 3′- and 2′-*O*-methoxyethyl modification. *Nucleic Acids Res.*, **31**, 2066–2076.
36. Egli,M. and Gessner,R.V. (1995) Stereoelectronic effects of deoxyribose O4′ on DNA conformation. *Proc. Natl Acad. Sci. USA*, **92**, 180–184.

37. Frederick,C.A., Coll,M., van der Marel,G.A., van Boom,J.H. and Wang,A.H.J. (1988) Molecular structure of cyclic deoxydiadenylic acid at atomic resolution. *Biochemistry*, **27**, 8350–8361.
38. Lapham,J., Rife,J.P., Moore,P.B. and Crothers,D.M. (1997) Measurement of diffusion constants for nucleic acids by NMR. *J. Biomol. NMR*, **10**, 255–262.
39. Yang,X.Y., Sanghvi,Y.S. and Gao,X.L. (1997) Conformational studies of antisense DNA by PFG NMR. *J. Biomol. NMR*, **10**, 383–388.
40. Avizonis,D.Z. and Kearns,D.R. (1995) Kinetic and thermodynamic characterization of DNA duplex–hairpin interconversion for 2 DNA decamers – d(CAACGGGTTG) and d(CAACCCGTTG). *Biopolymers*, **35**, 187–200.
41. Wüthrich,K. (1986) *NMR of Proteins And Nucleic Acids*. John Wiley & Sons, NY.
42. Finger,L.D., Trantirek,L., Johansson,C. and Feigon,J. (2003) Solution structures of stem–loop RNAs that bind to the two N-terminal RNA-binding domains of nucleolin. *Nucleic Acids Res.*, **31**, 6461–6472.
43. Mihailescu,M.-R. and Marino,J.P. (2004) A proton-coupled dynamic conformational switch in the HIV-1 dimerization initiation site kissing complex. *Proc. Natl Acad. Sci. USA*, **101**, 1189–1194.
44. Hannoush,R.N., Min,K.-L. and Damha,M.J. (2004) Diversity-oriented solid-phase sythesis and biological evaluation of oligonucleotide hairpins as HIV-1 RT RNase H inhibitors. *Nucleic Acids Res.*, **32**, 6164–6175.